CISTI ICIST

Document Delivery Service
in partnership with the **Canadian Agriculture Library**

Service de fourniture de Documents
en collaboration avec **la Bibliothèque canadienne de l'agriculture**

THIS IS NOT AN INVOICE / CECI N'EST PAS UNE FACTURE

SUSAN SALHIA
IRC-LIBRARY
AECL
2251 SPEAKMAN DR
MISSISSAUGA, ON L5K 1B2
CANADA

ORDER NUMBER:	**CI-04886648-4**
Account Number:	FGH24244
Delivery Mode:	FTP
Delivery Address:	
Submitted:	2004/08/19 09:27:05
Received:	2004/08/19 09:27:05
Printed:	2004/08/19 16:03:40

Direct	Periodical	WWW Catalogue	CANADA
12			
$ 12.00			

Client Number:	ROBERT ION - SP/0480
Title:	**HEAT AND TECHNOLOGY = CALORE E TECNOLOGIA.**
DB Ref. No.:	IRN10373640
ISSN:	03928764
Vol./Issue:	10,
Date:	1992
Pages:	46-74
Article Title:	TWO-PHASE FLOW REGIMES AND ONSET OF FLOW STRATIFICATION IN HORIZONTAL 37-ROD BUNDLES
Article Author:	OSAMUSALI, S.E., GROENVELD, D.C., CHENG, S.C
Report Number:	IRN10373640
Publisher:	PITAGORA EDITRICE,
Information Source:	INNOPAC

Estimated cost for this 31 page document: $11.4 document supply fee + $0 copyright = $11.4

Phone/Téléphone: 1-800-668-1222 (Canada - U.S./E.-U.) (613) 998-8544 (International)
www.nrc.ca/cisti Fax/Télécopieur: (613) 993-7619 www.cnrc.ca/icist
info.cisti@nrc.ca info.icist@nrc.ca

National Research Council Canada Conseil national de recherches Canada

HEAT and TECHNOLOGY
CALORE e TECNOLOGIA
Vol. 10 • No. 1-2 • 1992

TWO-PHASE FLOW REGIMES AND ONSET OF FLOW STRATIFICATION IN HORIZONTAL 37-ROD BUNDLES

S.I. Osamusali (*)(♦), D.C. Groeneveld (**)(♦), S.C. Cheng (♦)

ABSTRACT

Experiments have been conducted in a string of horizontal 37-rod bundles to determine the onset of flow stratification and the conditions under which the top element of the 37-rod bundle becomes completely dry around its periphery (i.e., onset of peripheral dryout or OPD). The experiments were performed with air-water flow at room temperature and atmospheric pressure, at mass fluxes up to 3000 kg/m^2s, and qualities up to 3.2%. The flow regimes in the horizontal 37-rod bundles were characterized from the waveform signals of the instrumented top element, and the void distributions were measured with a miniature fibre-optic probe. Effects of geometry and bundle misalignment were also investigated. The results were analyzed using dimensionless coordinates and extrapolated to other fluid and flow conditions. The mass fluxes and qualities corresponding to OPD in steam-water flow for pressures up to 20 MPa have been predicted for 37-rod bundles. The results show that flow stratification occurred at higher mass fluxes in rod bundles than in pipes. The rod-bundle void distributions show the same general trend as those of pipes but exhibit local variations at locations below the narrow element gaps, at the upper part of the subchannels. This seems to suggest bubble crowding, prior to the bubbles passing through the narrow gaps. No significant effects of bundle misalignment on the void distributions were observed.

(♦) Department of Mechanical Engineering, University of Ottawa, Ottawa, Ontario, Canada K1N 6N5.
(*) Present address: Ontario Hydro, 700 University Avenue, Toronto, Canada M5G 1X6.
(**) Chalk River Nuclear Laboratories, Atomic Energy of Canada Limited, Chalk River, Ontario, Canada K0J 1J0.

1. INTRODUCTION

1.1 General

In engineering designs of gas-liquid flow systems, it is important to predict the particular flow regime and the flow-regime transition boundaries. Design parameters such as heat and mass transfer rates and pressure drop can be more accurately determined if the flow regime is known. For example, in the primary heat transport system of a nuclear power plant, different flow regimes can be encountered in the flow channel. This could lead to significant changes in the heat transfer characteristics, pressure drop and critical heat flux (CHF).

In spite of the considerable effort in two-phase-flow research during the past two decades, the phase distribution in horizontal and inclined flows, with or without heat addition, is still not fully understood. The particular case of horizontal flow systems is complicated by flow stratification at low mass fluxes due to gravitational effects. Horizontal and inclined two-phase-flow effects are of paramount importance in CANDU* reactor fuel channels, boilers and piping, and in the chemical and process industry. Mechanistic models [1,2,3], a numerical approach [4] and empirical correlations [5,6] have all been developed for predicting the transitions from stratified to slug flow in horizontal pipes. Taitel and Dukler [1] developed a model for predicting the transition between stratified and intermittent or annular/wavy-annular flows in pipes, based on the Kelvin-Helmholtz instability criteria for wave growth at the gas-liquid interface. They obtained the transition criteria by considering the destabilizing force on a solitary wave resulting from a reduction in the pressure over the wave crest, and the stabilizing force due to gravity. The critical condition where this transition occurs is attained when these forces cancel out.

So far, most studies on flow stratification have dealt with tube flow, with only a few studies reported for rod bundles. Krishnan and Kowalski [7] have derived transition criteria from stratified to slug flow in rod bundles using an energy-balance approach. They derived empirical expressions for the interfacial perimeter and void fraction required for predicting flow stratification, for horizontal rod-bundles.

*CANDU - CANada Deuterium Uranium. A registered trademark of Atomic Energy of Canada Limited.

Osamusali and Chang [8] adopted the approach of Taitel and Dukler [1], theoretically deriving equations for the interfacial area and void fraction for flow stratification in rod bundles.

The objectives of the present study are:

(i) to determine the flow-regime boundaries of a horizontally oriented 37-rod bundle,

(ii) to define the flow threshold beyond which the top-element periphery becomes completely dry (i.e., onset of peripheral dryout (OPD)),

(iii) to provide typical flow-regime map and void distributions for rod bundles.

1.2 Flow Regimes

Various classifications of the different flow regimes observed in horizontal flows have been reported. The descriptions of two-phase flow patterns occurring in rod bundles have been observed to be similar to those of pipes [8]. However, slight variations from the flow-regime descriptions for pipes have been observed by Aly [9] for rod-bundle subchannels. Four different classifications are generally accepted for co-current gas-liquid flow in horizontal channels. These flow structures are defined below and illustrated in Fig. 1.

(i) **Stratified Flow**: The stratified flow regime is characterized by the liquid flowing at the bottom of the pipe and the gas on top, separated by an interface. The case with a smooth gas-liquid interface is referred to as stratified smooth flow. At high gas-flow rates, the gas-liquid interface may become wavy, leading to the stratified wavy flow regime. In rod bundles, interfacial waves may result from flow disturbances at the endplates.

(ii) **Intermittent Flow**: The intermittent flow regime is characterized by liquid bridging the gap between the gas-liquid interface and the top of the pipe. The liquid bridges are separated by stratified flow zones. The intermittent flow is subdivided into the plug flow regime, occurring at low gas velocities and having a liquid bridge free of gas bubbles, and the slug flow regime, which occurs at higher gas-flow rates and entrains a significant amount of gas bubbles in the liquid bridge. During intermittent flows in rod bundles, the liquid bridges across the elements at the upper part of the channel.

(iii) **Annular Flow**: The annular flow pattern is characterized by the liquid phase flowing around the inner periphery of the pipe and surrounding a core of fast-flowing gas phase. The gas core may entrain some liquid droplets, and the gas-liquid interface is generally wavy. At low gas-flow rates, the liquid essentially flows as a thick film at the bottom of the pipe with rather unstable waves at the gas-liquid interface, continuously swept up around the pipe periphery, resulting in the wavy-annular flow regime. This eventually leads to the fully developed annular flow regime at higher gas-flow rates, characterized by a continuous liquid film around the inner periphery of the pipe. During annular flows, the rod-bundle elements in the gas core may be covered with very thin liquid films.

(iv) **Bubbly Flow**: The bubbly flow regime is characterized by the void being in the form of discrete bubbles, which are distributed throughout the continuous liquid phase that otherwise fills the pipe section. The bubble concentration is highest at the top of the pipe, especially at the lower mass velocities.

2. DESCRIPTION OF EXPERIMENTAL EQUIPMENT

2.1 MR-2 Experimental Facility

The MR-2 experimental facility is a multipurpose single-phase and two-phase air-water rig with a recirculating water flow section. A globe valve located downstream of the test section is used to adjust the exit pressure. The water is pumped by a centrifugal pump driven by a 15 hp induction motor. The water-flow rate is measured using a turbine flow meter for flow rates up to 2.0 kg/s, and an orifice meter for higher flow rates. The water-flow rate is regulated with a Bailey Controller, which operates two regulating valves, connected in parallel, for high and low flow rates. Air-flow rates up to 0.026 kg/s were measured with two rotameters connected in series. The air is supplied from a central compressor. The air and water flow through a mixing section, consisting of flow-straightening tubes, and their temperatures are monitored using thermocouples. A schematic representation of the MR-2 loop is shown in Fig. 2.

2.2 Experimental Test Section

The MR-2 test section is a 244-cm-long transparent Lucite tube, of 10.34 cm inside diameter. The tube encloses a string of four CANDU, 37-rod bundles. The spacings between the rods are maintained by mid-plane spacers and two endplates, as shown in Fig. 3. A series of thirty pressure taps are in place for axial pressure-drop measurements, and a set of six bubble-injection ports is located at the bottom of the tube, upstream of the fibre-optic probe. The third bundle downstream from the inlet consists of 37 empty Zircaloy fuel sheaths simulating CANDU fuel rods and serves as the test bundle for this study.

2.3 Instrumented Top Element

The top element of the test bundle is instrumented for detecting the presence of a liquid film on the element from resistance measurements, and hence determining the onset of complete flow stratification (i.e., OPD). It consists of four sections of Zircaloy tubes joined together by sections of insulator material (Teflon) having the same outer diameter of 1.3 cm as the Zircaloy tubes simulating the CANDU fuel rods. A schematic diagram of the top element and the circuitry for electrical resistance measurement is shown in Fig. 4. The end caps of the instrumented element are also made of insulator materials (Lucite) to isolate it electrically from the rest of the bundle. The presence of a conducting fluid (water) on the top element can be detected by measuring the electrical resistance across the insulator sections, hence determining the conditions under which the top element becomes completely dry.

2.4 Twin-Needle Fibre-Optic Probe

A twin-needle fibre-optic probe is located 40 cm from the upstream endplate of the test bundle. The bundle is 50 cm long. A narrow slit, 2 mm wide, in the centre element of the test bundle enables the fibre-optic probe to traverse across the bundle, for measurement of the lateral void distribution. The principle of operation of a fibre-optic probe is based on Snell's law applied at the tip location. Depending on the particular phase surrounding the tip, the incident light may be completely reflected (for an air-glass interface) or completely transmitted (for a water-glass interface). The twin-needle fibre-optic probe used in the present experiment has two Y-junction glass fibres. The base of the Y is the needle portion of the probe, and the two legs represent the transmitter and receiver ends. The probe consists of a triangular-shaped stem, made of stainless steel, and two small tubes inserted into the rounded edge of the triangular stem at the base. The small tubes are constructed with stainless steel, 0.5 mm outer diameter. These are then bent into an L-shape, and placed side by side, with the fibres exposed at the tip of the probe. The tip of the short needle is separated from the long needle tip by about 1.2 mm, and the needles are spaced about 0.5 mm apart. A schematic of the fibre-optic probe is shown in Fig. 5.

2.5 Signal Processing

The received signals are fed into photodiodes which convert them to electronic signals. A trigger level to discriminate the air and water was adjusted manually in the comparator, and signals below this threshold value are considered to be noise or purely water signals. The signals corresponding to the void are considerably higher than the threshold, so that high sensitivity can still be achieved. For void fraction measurements, signals from the long needle which encounters the gas phase first are fed into an AND gate along with a 1 MHz clock signal (i.e., the presence of the vapour phase is detected at a sampling rate of 1 MHz). Whenever the needle tip is in contact with the gas phase, the signals will be high and a counter is incremented. At the end of the sampling time, the local time-averaged void fraction is calculated by dividing the amount of time that the tip was in contact with gas by the total sampling time. The output appears as a percentage on an LED display.

3. EXPERIMENTAL PROCEDURE

3.1 General

In this study, the flow regimes and flow-regime boundaries for 37-rod bundles were first determined. This was achieved by direct visual observation through the transparent test section, and from output signals of the instrumented top element. Void distributions in the rod bundle were obtained by traversing the fibre-optic probe across the bundle and measuring the time-average local void fractions at forty radial positions. The onset of flow stratification was determined using the instrumented top element in the test bundle. In this procedure, the air-flow rate was fixed and the water-flow rate set to correspond to intermittent flow. At this flow condition, liquid bridges occur very frequently across several rod-bundle elements, causing the top element to be continuously wet. A reduction in the liquid-flow rate decreases the frequency of occurrence of the liquid bridges, and the top element becomes intermittently dry (i.e., onset of intermittent dryout or OID). The water-flow rate was then reduced gradually until complete flow stratification was observed. Again, direct visual observation and the signals from the instrumented top element were used to determine when the flow was fully stratified. OPD was obtained when the electrical resistance across the insulating strip of the top element became infinite (i.e., the top element is completely dry around its periphery). The procedure was repeated for different values of the air-flow rate, until the annular/wavy-annular flow boundary was reached, where the top element became covered with a very thin liquid film.

These measurements were initially performed on a string of aligned 37-rod bundles, followed by some measurements with the upstream bundle junctions misaligned by 11.5°, which is the angle of misalignment found to yield the most pressure drop across the bundle junction.

4. EXPERIMENTAL RESULTS

4.1 Void Distribution

Typical void distributions corresponding to different flow regimes are presented in Fig. 6. Fig. 7 shows the radial void distributions for air-water flows in 37-rod bundles at mass fluxes ranging from 200 kg/m^2s to 3000 kg/m^2s, and qualities up to 3.2%. In this figure, the data for aligned bundles are plotted in shaded symbols and joined by solid lines, while the corresponding open symbols represent the case for misaligned bundles. The radial positions in the range $-0.12 \leq (r/R) \leq +0.12$ contain no useful data, since this range corresponds to the position occupied by the centre element.

4.2 Flow Regimes

The waveform signals of the instrumented top element, for different flow regimes, are shown in Fig.

8. About two hundred and twenty-five data points corresponding to stratified smooth, stratified wavy, plug, slug, bubbly and annular/wavy-annular flow regimes for aligned endplates and bundles have been plotted in different areas of the map, representing a combination of the superficial velocities at which the flow regimes occurred. The approximate locations of the transition boundaries between the flow regimes have been marked with lines. However, the experimental data points indicate that the flow-regime transitions are gradual rather than sudden, as may be implied by the lines. Fig. 10 shows the flow-regime results for the 37-rod bundles analyzed as above, but uses the total mass flux, G, and the flow quality, x, as coordinates.

From the results of Fig. 8, stratified flow regimes occurring at low liquid-flow rates were obtained when the instrumented top element signal became flat. In this case, the top element remained completely dry around its periphery, since the gas-liquid interface is not high enough to touch this rod-bundle element. The intermittent flow regimes (plug and slug) were obtained at higher liquid-flow rates when the instrumented top elements yielded fluctuating signals. The fluctuations in this case are inverted since the liquid suddenly loses contact with the top element leaving a liquid bridge to flow through the channel. This is clearly depicted by the slug flow signals, where the fluctuations seem to occur at irregular intervals, and the liquid is seen to lose complete contact with the top element as the slug of liquid flows through the channel. The small amplitude fluctuations occurring periodically indicate the presence of plugs of elongated bubbles flowing through the channel, while the liquid partially maintains contact with the upper part of the channel. At low liquid-flow rates, large amplitude waves at the gas-liquid interface are continuously swept across the rods to the top of the channel by the fast flowing gas-phase. This causes the gas-liquid interface to intermittently wet the top element as indicated by the upright fluctuations of the signals. In this case, liquid droplets deposited on the rods and at the upper part of the tube are spread by the fast flowing gas phase, yielding very thin liquid films on both the rods and the channel wall, thus characterizing the wavy-annular flow regime. The bubbly flow regime occurs when the instrumented top element yields a flat signal with infinitesimal spikes, since in this case the liquid is flowing in the full channel cross-section with the gas flowing as dispersed bubbles.

4.3 Onset of Stratification

The results of the flow stratification experiment have been combined with the flow-regime data plotted in Figs. 9 and 10. Flow stratification is observed to occur at the transitions from plug, slug and wavy-annular flow regimes. The conditions for the onset of stratification at the plug and slug flow transitions appear to be independent of the gas-flow rate, as shown in Fig. 9. This corresponds to a superficial liquid velocity of about 0.14 m/s, for a wide range of gas-flow rates. However, a slight dependence of onset of stratification on flow quality at the transition to plug flow exists. The mass flux at the transition to annular/wavy-annular flow appears to decrease with quality, as shown in Fig. 10.

5. DISCUSSION

5.1 Void Distribution

The void distributions for 37-rod bundles at various gas- and liquid-flow rates have been presented in Figs. 6 and 7, for both aligned and misaligned bundles. The results show that for a mass flux of 574.3 kg/m^2s and quality of 0.10%, the liquid film at the bottom of the channel is thicker than the tube radius. The plug flow regime was observed to occur at this flow condition. Fig. 6b shows that the liquid film in plug flow does not entrain any gas bubbles, hence the flow at the bottom half of the channel is mainly single phase water. At a quality of 0.46%, slug flow occurs, having liquid films less than the tube radius (see Figs. 6c and 7b). At higher qualities, the liquid film at the bottom of the channel is much less than the tube radius (see Fig. 6d). At these flow conditions, annular/wavy-annular flows occur, also having thin liquid films at the top of the channel. At a high mass flux of 2870 kg/m^2s, for qualities up to 0.09%, bubbly flow regimes were observed, as shown in Fig. 7d. The results show that in bubbly flows, gas bubbles are also entrained in the liquid films below the centre of the channel.

In general, the local void fractions are higher at the top of the channel than at the bottom, with significant effects of stratification noticeable for plug, slug and bubbly flows.

5.1.1 <u>Effect of Geometry:</u> The void distributions also show significant local variations caused by the rod-bundle geometry (see Figs. 6 and 7). These local variations in the void distributions peaked at locations below the narrow element gaps at the upper part of the subchannels. This indicates bubble crowding prior to the bubbles passing through the narrow element gaps. This bubble crowding, due mainly to the rod-bundle geometry, could lead to a lower CHF for the narrow gap region. This is also the reason for slight differences in the flow-regime structures of tubes and bundles.

5.1.2 **Effect of Channel Orientation:** Lahey and Schraub [10] reviewed a similar experiment, conducted by Kangas and Neusen [11] for steam-water flow in a vertical 16-rod bundle, using the gamma-ray attenuation technique. The results for mass flux of 1670 kg/m^2s, quality of 0.82% and heat flux of 498 kW/m^2 showed local variations in the void distributions. The local void fractions (chordal average) peaked in the region of interior subchannels and were lower in the rod gaps. The radial void distribution for the 16-rod bundle vertical flow were symmetric across the bundle. However, the void distributions for 37-rod bundle horizontal flows, investigated here, also showed local variations but were asymmetric across the bundle. Unlike the vertical flow case, the local void fractions for the horizontal rod-bundle flow peaked at locations below the rod gaps at the upper part of the subchannels, and were lower at the bottom of the subchannels (see Figs. 6 and 7). Hence, for interior subchannels of a horizontal rod-bundle, the void distributions are asymmetric, with a higher void fraction at the top of the subchannels. This is similar to horizontal pipe flow cases (except fully dispersed bubbly flows), and shows that gravitational effects are still dominant within subchannels. The present results can be of direct application in the subchannel analysis of horizontal rod-bundle flows.

5.1.3 **Effect of Bundle Misalignment:** In general, the effects of bundle misalignment on void distributions were insignificant in these experiments, as shown in Fig. 7. This was surprising, as it was expected that improved mixing due to misalignment would homogenize the flow, lower the slip ratio, and hence increase the void fraction. However, the flows achieved here might not have been high enough to obtain this condition.

5.2 Flow-Regime Map

A generalized flow-regime map for horizontal 37-rod bundles has been obtained based on air-water experimental data at room temperature and near atmospheric pressure. The results have been compared with the theoretical prediction of Taitel and Dukler's model for pipes [1].

5.2.1 <u>Dimensionless Representation:</u> The dimensionless quantities, X, F, and T, originally proposed by Taitel and Dukler [1], have been used here. These quantities were obtained from a theoretical modelling of the flow-regime transitions from physical mechanisms. The flow regimes considered, which were also characterized in the 37-rod bundle geometry, are the stratified (stratified smooth and stratified wavy), intermittent (plug and slug), annular/wavy-annular and bubbly flows. The relative areas occupied by each flow regime are shown in Fig. 11.

The dimensionless parameter, X, is the one defined by Lockhart and Martinelli [12],

$$X=\sqrt{\left(\frac{(dp/dx)_{LS}}{(dp/dx)_{GS}}\right)} \qquad (1)$$

where $(dp/dx)_{LS}$ represents the pressure drop with the liquid phase flowing alone in the channel, and $(dp/dx)_{GS}$ represents the pressure drop with the gas phase flowing alone in the channel. The parameter, X, can be expressed for 37-rod bundles as a function of the superficial velocities in the form,

$$X=\left(\frac{\mu_L}{\mu_G}\right)^{0.108}\left(\frac{\rho_L}{\rho_G}\right)^{0.392}\left(\frac{U_{LS}}{U_{GS}}\right)^{0.892} \qquad (2)$$

where U_{LS} and U_{GS} are the superficial velocities of the liquid and gas phases, respectively. The superficial velocity represents the case when the gas or the liquid is assumed to be flowing alone in the channel. For rod bundles, the superficial velocity is based on the channel cross-sectional area excluding the area occupied by the rods. The above expression has been obtained using a friction factor correlation developed for bare 37-rod bundles, namely, $f=0.243Re^{-0.216}$, where Re is the Reynolds number based on hydrodynamic diameter. Substituting for the superficial velocities with the total mass flux, G, and the flow quality, x, in Eq. (2), the parameter, X, can be expressed for 37-rod bundles as,

$$X=\left(\frac{\mu_L}{\mu_G}\right)^{0.108}\left(\frac{\rho_G}{\rho_L}\right)^{0.5}\left(\frac{1-x}{x}\right)^{0.892} \tag{3}$$

Hence, X can be calculated with the knowledge of the flow rates, fluid properties, tube diameter and rod-bundle element diameter.

The dimensionless parameter, F, is the modified Froude number, which was obtained from a consideration of the dominant mechanisms in the stratified to intermittent or annular transition. This is given as,

$$F=\sqrt{\left(\frac{\rho_G}{(\rho_L-\rho_G)gD_{hy}}\right)}U_{GS} \tag{4}$$

where D_{hy} is the hydrodynamic diameter, obtained based on the channel cross-sectional area, excluding the area occupied by the rods, and the total wetted perimeter of both the rods and the channel wall. F can be expressed in terms of the total mass flux, G, and the flow quality, x, as,

$$F=\frac{Gx}{\sqrt{(\rho_G(\rho_L-\rho_G)gD_{hy})}} \tag{5}$$

F can be easily calculated from known physical quantities and flow parameters.

dominant forces in the intermittent to bubbly flow transition. T is given as,

$$T=\frac{(dp/dx)_{LS}}{\sqrt{(\rho_L-\rho_G)g}} \tag{6}$$

T can also be expressed in terms of superficial velocities as,

$$T=\left(\frac{2\rho_L C_L}{(\rho_L-\rho_G)gD_{hy}}\right)^{0.5}\left(\frac{\mu_L}{\rho_L U_{LS} D_{hy}}\right)^{0.108} U_{LS} \tag{7}$$

where C_L=0.06075 (from the 37-rod bundle friction-factor coefficient of 0.243), and D_{hy}=7.6 mm (corresponding to the 37-rod bundle geometry). The parameter T can further be expressed in terms of the total mass flux and the flow quality, x, as,

$$T=\left(\frac{2C_L}{\rho_L(\rho_L-\rho_G)gD_{hy}}\right)^{0.5}\left(\frac{\mu_L}{(1-x)GD_{hy}}\right)^{0.108} G(1-x) \tag{8}$$

5.2.2 Flow-Regime Transition Boundaries: The flow-regime results presented in the previous section have been replotted on a Taitel and Dukler type flow-regime map, as shown in Fig. 11. The flow-regime transition boundaries A, A', B and D, have been obtained by plotting F versus X for A and A', and T versus X for D and X=1.6 for line B. In the present analysis, the results for the stratified and intermittent or annular flow regimes have been analyzed by plotting coordinate F versus X, with the axis numbers on the left, while only the bubbly flow regime was analyzed by plotting coordinate T versus X, with the axis numbers on the right of the figures. The curves labelled A, B and D are the theoretical predictions of

Taitel and Dukler's model for pipes [1]. Curve A' is the experimental transition boundary between stratified and intermittent or annular flow for 37-rod bundles. The rod-bundle results shown with data symbols have been obtained experimentally for air-water flow at room temperature and near atmospheric pressure. The results show that the transition from stratified to intermittent flows in 37-rod bundles (D_{hy} = 7.6 mm), represented by curve A', occurs at higher mass fluxes than the case for pipes, represented by curve A. Dukler and Taitel [13] have stated that the pipe results are independent of diameter. In the present analysis, the difference obtained in the stratified to intermittent transition for pipes and rod bundles may therefore be attributed to other geometrical effects, such as endplates and spacers. The intermittent to bubbly flow transition for pipes represented by curve D seems to give a good prediction of the rod-bundle flow results, since all the data lie above this curve. Curve B represents the transition boundary between annular and intermittent or bubbly flows, and seems to give a good prediction of the rod-bundle results, since both the intermittent and the bubbly flow data lie to the right of this curve. The rod-bundle data for wavy-annular flow is not well predicted by curve B. The wavy-annular flow is, however, a transitional flow regime from the intermittent to the fully developed annular flow.

Fig. 12 shows the generalized flow-regime map for pipes and rod bundles in solid lines, while the dashed lines are those obtained by plotting T or F versus X for steam-water flow, and for mass fluxes ranging from 50 kg/m^2s to 6000 kg/m^2s, at a pressure of 10 MPa. The results show that for steam-water flow at 10 MPa, the mass flux for the stratified to intermittent or annular transition ranges from about 50 kg/m^2s to 150 kg/m^2s. This result is useful for determining the conditions for OPD in horizontal 37-rod bundles. The curves for higher mass fluxes, of up to 250 kg/m^2s, correspond to cases of partial stratification due to plug, slug and annular/wavy-annular flow regimes, and coincide with the OID condition. The intermittent to dispersed bubbly flow transition for a 10 MPa steam-water flow in 37-rod bundles, occurs for mass fluxes ranging from 1000 kg/m^2s to 2000 kg/m^2s.

5.3 Onset of Stratification

5.3.1 <u>Comparison of Data with Predictions:</u> Compared to the flow-regime map of Taitel and Dukler [1], the onset of complete flow stratification in 37-rod bundles (D_{hy}=7.6 mm), was found to occur at a higher mass flux than for the pipe case (see Fig. 12). At high qualities, parameter $X \leq 0.1$, the results for both pipes and rod bundles tend to converge to the condition, F=1. Physically, this is the condition where the inertial forces of the gas phase and the gravitational force acting on the liquid are balanced. At this flow condition, fully developed annular flow exists, where the liquid swept to the top of the pipe is sustained, hence maintaining a continuous liquid film around the pipe periphery.

5.3.2 **CHF Boundaries for Horizontal 37-Rod Bundles:** The onset of stratification conditions for steam-water flow in 37-rod bundles has been presented as a function of the total mass flux and quality at various pressures in Fig. 13. These conditions also define the flow threshold beyond which the top element becomes completely dry around its periphery. The assumption made was that extrapolation from the present air-water data obtained for 37-rod bundles to steam-water flows is possible using the dimensionless coordinates of the Taitel and Dukler flow-regime map [1]. The results show that the mass flux at the onset of flow stratification increases with pressure at high qualities, and tends to decrease with increasing pressure, at low qualities. The region of increasing mass flux, at high qualities, corresponds to that where transition from stratified to annular/wavy-annular flow occurs, while the region of decreasing mass flux, at low qualities, corresponds to that where transition occurs from stratified to slug or plug flow.

6. CONCLUSIONS AND FINAL REMARKS

The void distributions, flow regimes, and conditions for onset of flow stratification in 37-rod bundles have been investigated experimentally. The effects of geometry, flow rates, and bundle misalignment were discussed, and the following has been concluded:

(1) The flow-regime descriptions in rod bundles are, in general, similar to those of pipes, except for some local variations in the rod-bundle void distributions due to the geometry.

(2) In the rod-bundle geometry, bubbles appear to accumulate in the region below the narrow element gaps at the upper part of the subchannels thus causing partial flow stratification within a subchannel.

(3) No obvious effects of bundle misalignment on void distributions were observed for all flow regimes in the mass flux range of 200 to 3000 kg/m^2s.

(4) There is a significant effect of geometry on the onset of complete flow stratification. The onset of complete flow stratification for 37-rod bundles was found to occur at higher mass fluxes than predicted for pipes.

(5) The onset of complete flow stratification was observed to coincide with the onset of peripheral dryout for the top element of the 37-rod bundle.

(6) The mass flux at the onset of complete flow stratification was observed to depend on quality: at low qualities the maximum mass flux for stratified flow (before it changes into slug flow) is considerably higher than at higher qualities, where stratified flow changes into annular flow.

NOMENCLATURE

C_L Constant in Eq. (7)

D_{hy} Hydraulic Diameter (m)

F Modified Froude Number Defined in Eq. (4)

G Total Mass Flux (kg/m^2s)

g Gravitational Acceleration (m/s^2)

p Pressure (N/m^2)

T Dimensionless Force Defined in Eq. (6)

U_{LS} Superficial Liquid Velocity (m/s)

U_{GS} Superficial Gas Velocity (m/s)

X Dimensionless Parameter Defined in Eq. (1)

x Flow Quality

Greek Symbols

α Void Fraction

μ_L Liquid Viscosity (kg/m.s)

μ_G Gas Viscosity (kg/m.s)

ρ_L Liquid Density (kg/m^3)

ρ_G Gas Density (kg/m^3)

σ Surface Tension (N/m)

Subscripts

G, g Gas

GS Superficial Gas

hy Hydraulic

i Interface

L Liquid

LS Superficial Liquid

REFERENCES

(1) Y. Taitel and A.E. Dukler: A Model for Predicting Flow Regime Transitions in Horizontal and Near Horizontal Gas-Liquid Flow. AIChE J., Vol. 22, No. 1, pp 47 (1976).

(2) G.B. Wallis and J.E. Dobson: The Onset of Slugging in Horizontal Stratified Air-Water Flow. Int. J. Multiphase Flow, Vol.1 pp173 (1973).

(3) K. Mishima and M. Ishii: Theoretical Prediction of Onset of Horizontal Slug Flow. J. Fluids Eng., Vol. 102 pp441 (1980).

(4) A. Minato, T. Ikeda and M. Naitoh: Mechanistic Model of Slugging Onset in Horizontal Circular Tubes. J. Nucl. Sci. and Tech., Vol. 23, No. 9 pp761 (1986).

(5) J.M. Mandhane, G.A. Gregory and K. Aziz: A Flow Pattern Map for Gas-Liquid Flow in Horizontal Pipes. Int. J. Multiphase Flow, Vol. 1 pp537 (1974).

(6) J. Weisman, D. Duncan, J. Gibson and T. Crawford: Effects of Fluid Properties and Pipe Diameter on Two-Phase Flow Patterns in Horizontal Lines. Int. J. Multiphase Flow, Vol. 5 pp437 (1979).

(7) V.S. Krishnan and J.E. Kowalski: Stratified-Slug Flow Transition in a Horizontal Pipe Containing a Rod Bundle. AIChE Symposium Series, No. 238, Vol. 80 pp282 (1984).

(8) S.I. Osamusali and J.S. Chang: Regime-4 Code for Prediction of Flow Regime Transitions in a Horizontal Pipe, Annulus and Rod Bundle Flow Under Gas-Liquid Two-Phase Flow. Proc. 8th Annual Can. Nucl. Soc. Conf. Saint John, NB. (1987).

(9) A.M.M. Aly: Flow Regime Boundaries for an Interior Subchannel of a Horizontal 37-Element Bundle. Can. J. Chem. Eng.Vol. 59, No. 2, pp158 (1982).

(10) R.T. Lahey and F.A. Schraub: Mixing, Flow Regimes, and Void Fraction for Two-Phase Flow in Rod Bundles. ASME Winter Annual Mtg., Los Angeles, CA., November 1969.

(11) G. Kangas and K. Neusen: Pressure Drop and Void Fraction Experiments in Simulated Pathfinder Boiler Fuel Elements. ACNP-63002, March 1963.

(12) R.W. Lockhart and R.C. Martinelli: Proposed Correlation of Data for Isothermal Two-Phase, Two-Component Flow in Pipes. Chem. Eng. Progress Vol. 45 pp537.

(13) A.E. Dukler and Y. Taitel: Flow Pattern Transitions in Gas-Liquid Systems: Measurement and Modelling. Multiphase Science and Technology, Eds. G.F. Hewitt, J.M. Delhaye and N. Zuber, Vol. 2, pp1-94 (1987).

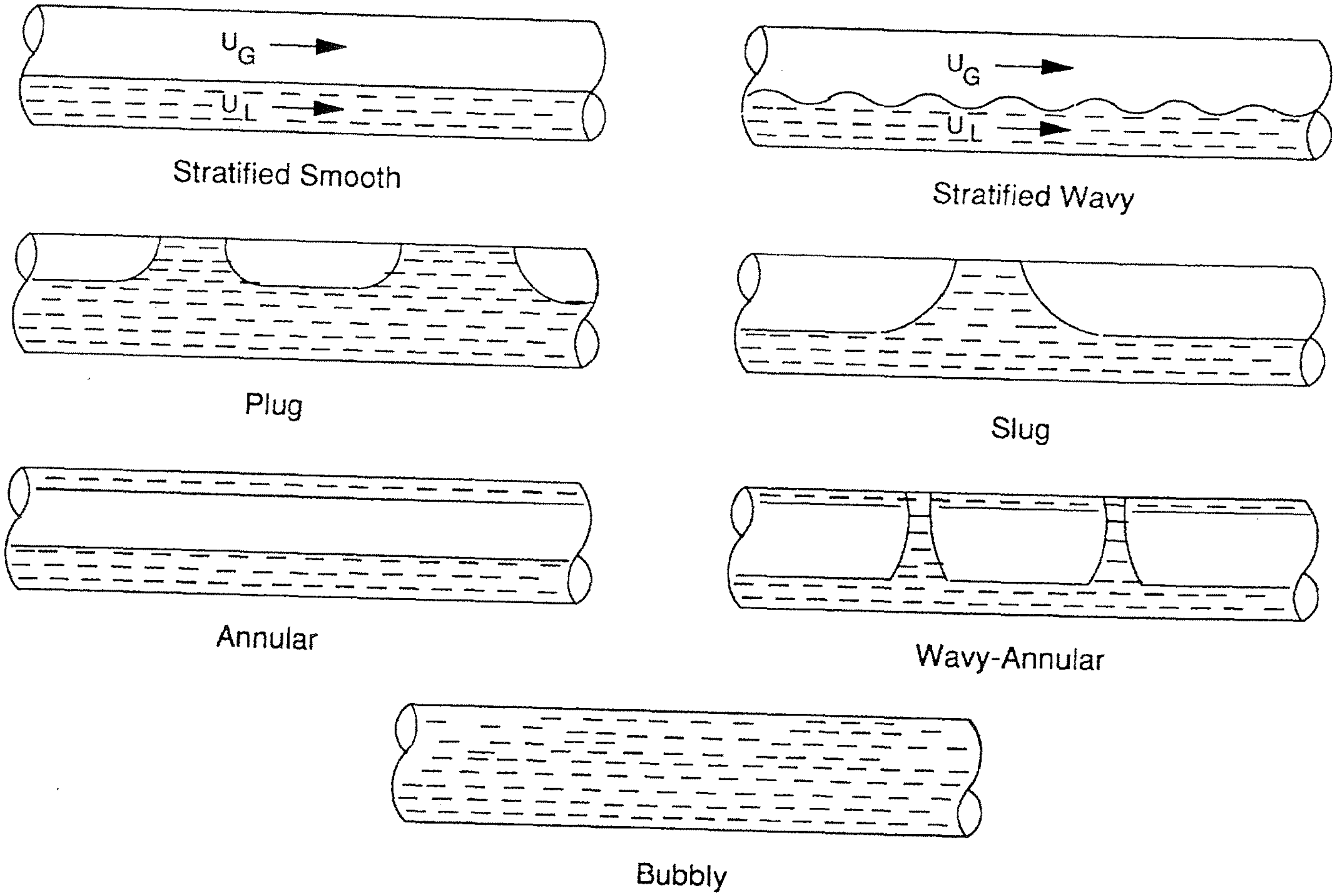

Figure 1: Two-Phase Flow Regimes for Horizontal Channels.

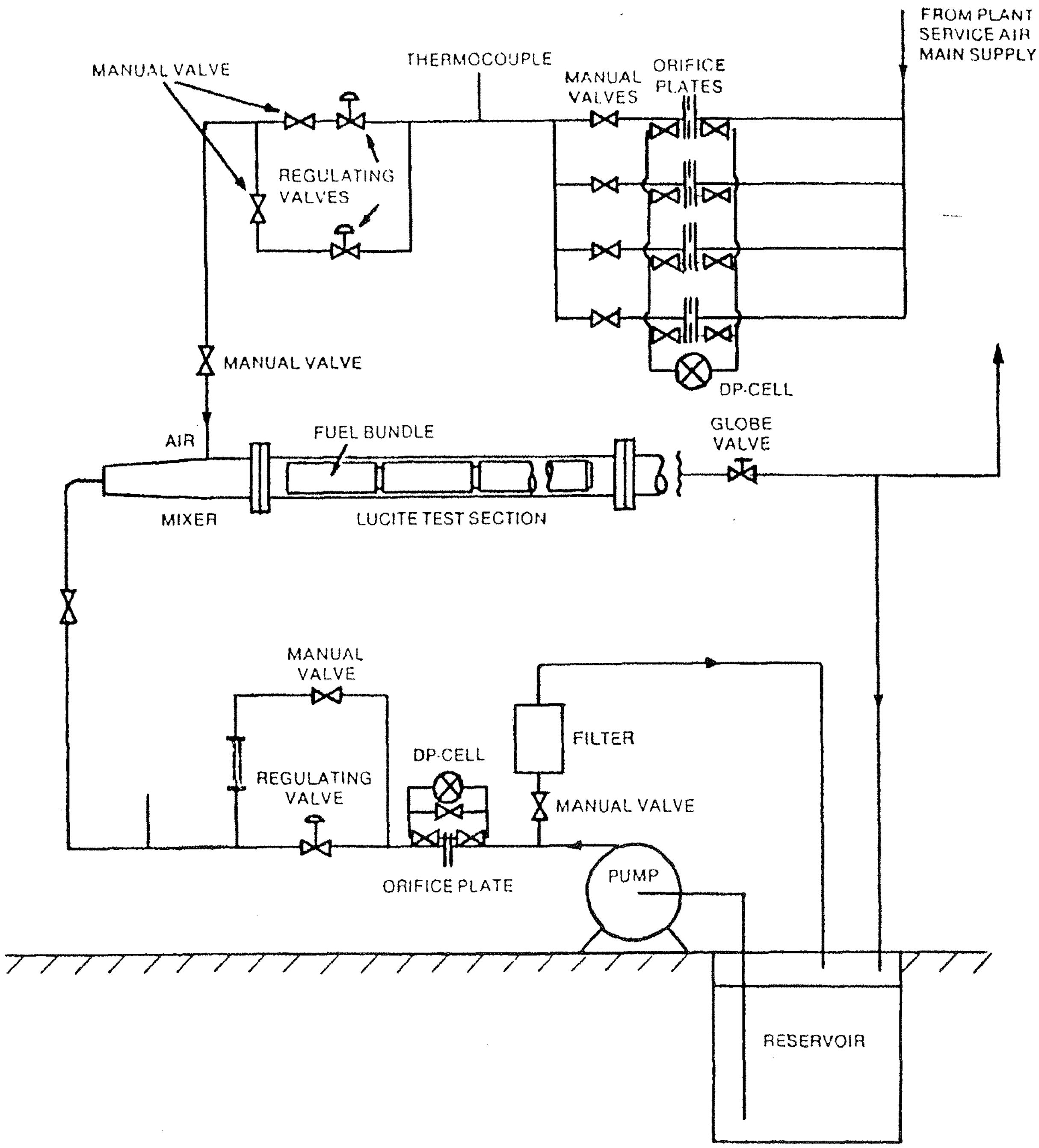

Figure 2: Schematic of MR-2 Experimental Facility.

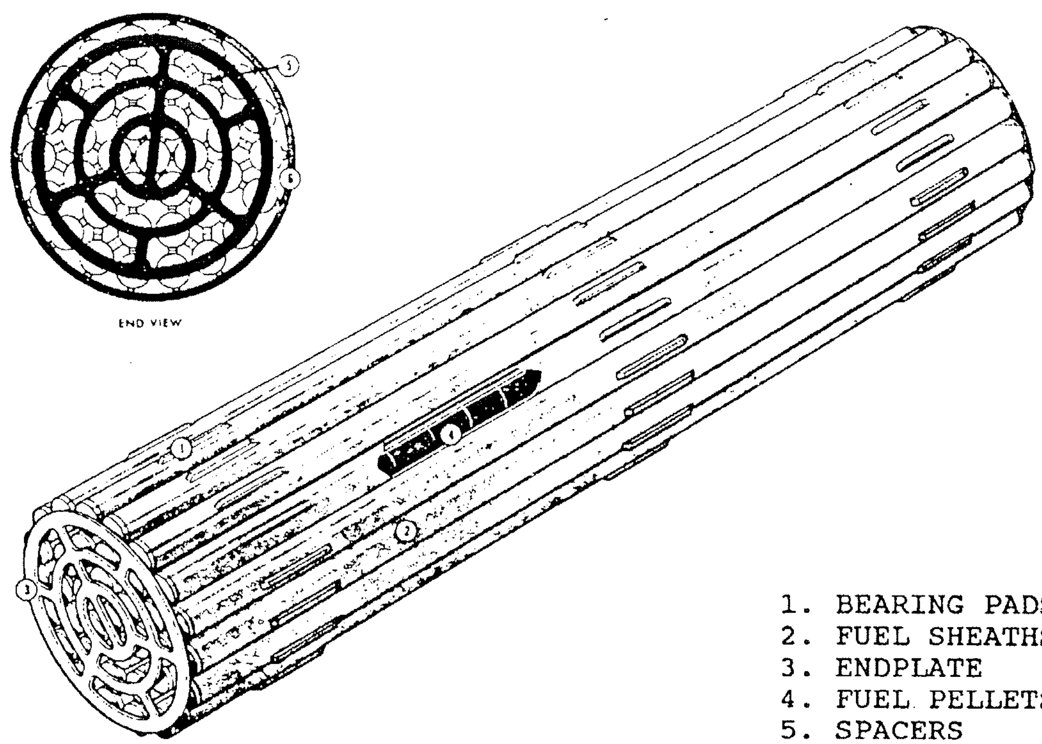

1. BEARING PADS
2. FUEL SHEATHS
3. ENDPLATE
4. FUEL PELLETS
5. SPACERS
6. PRESSURE TUBE

Figure 3: 37-Element Nuclear Fuel Bundle.

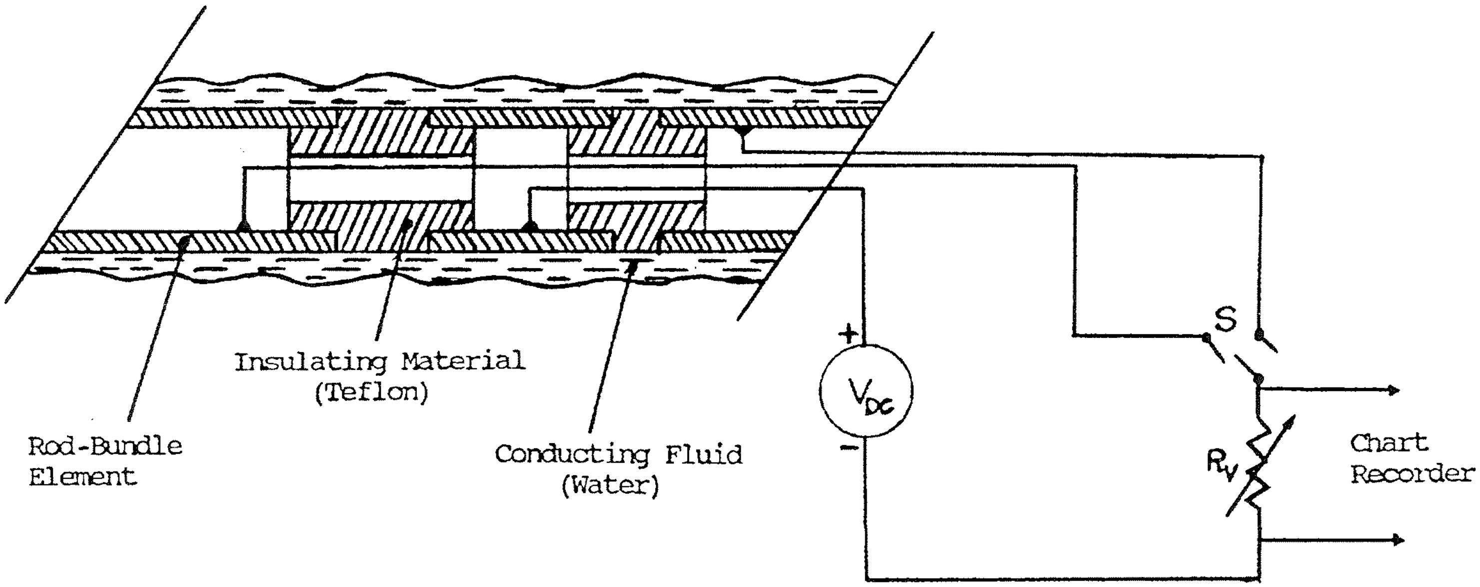

All dimensions are in mm.

S =Switch
R_V=Variable
Resistor

Figure 4: Schematic of Instrumented Top Element and Circuitry for Electrical Resistance Measurement.

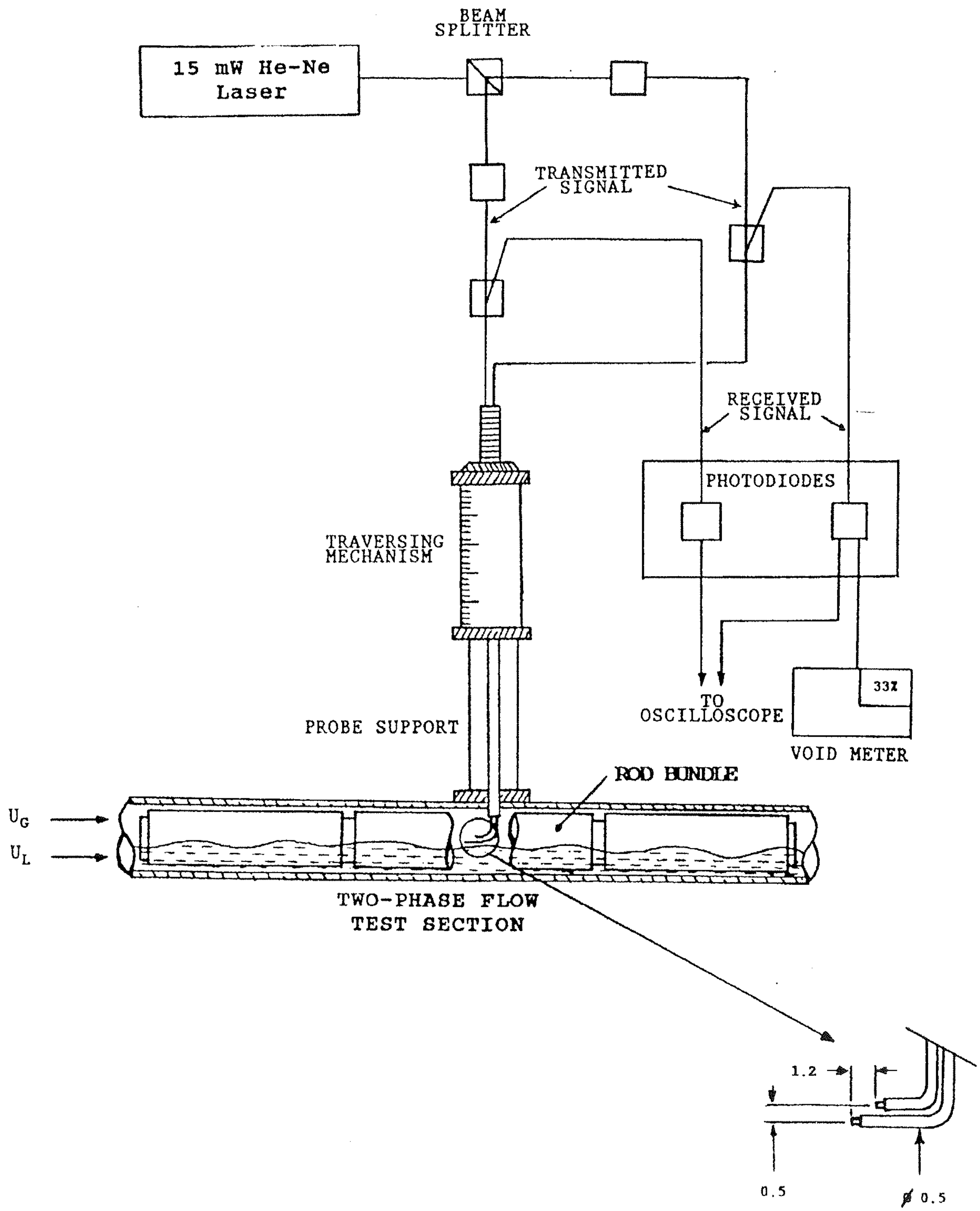

Figure 5: Set-Up of Twin-Needle Fibre-Optic Probe.

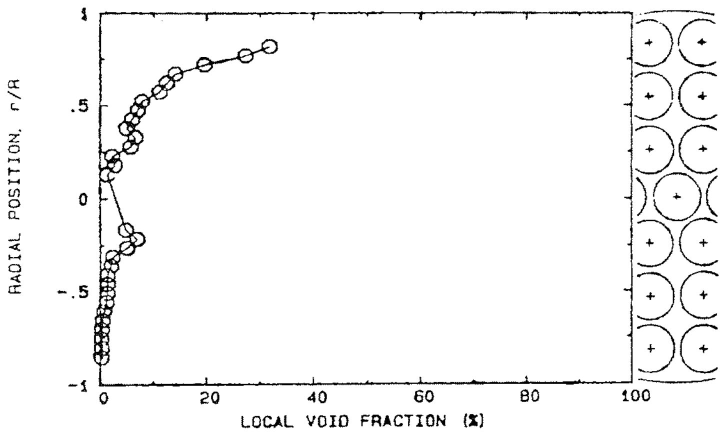

(a) BUBBLY FLOW REGIME
(G=2869 kg/m^{2}s; x=0.02%)

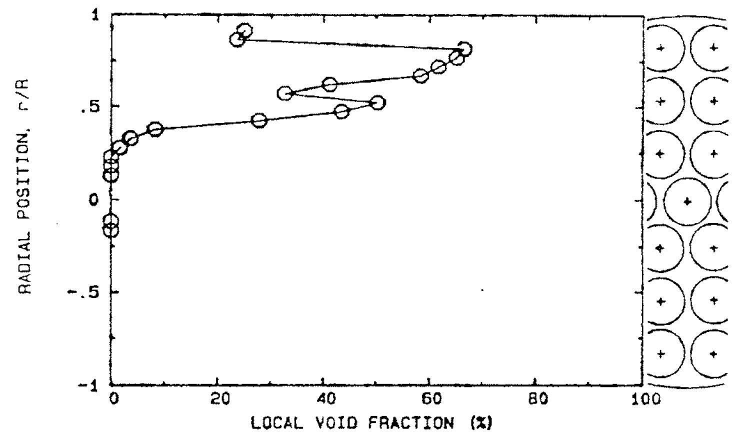

(b) PLUG FLOW REGIME
(G=574.3 kg/m^{2}s; x=0.10%)

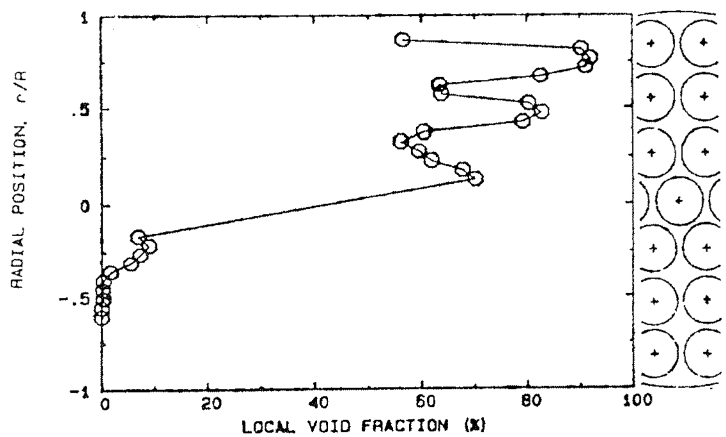

(c) SLUG FLOW REGIME
(G=576.4 kg/m^{2}s; x=0.46%)

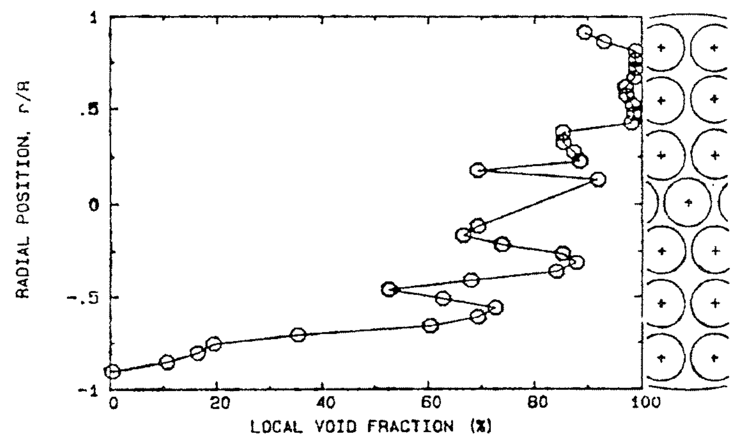

(d) WAVY-ANNULAR FLOW REGIME
(G=222.2 kg/m^{2}s; x=3.2%)

Figure 6: Void Distributions of Different Flow Regimes in Horizontal 37-Rod Bundles.

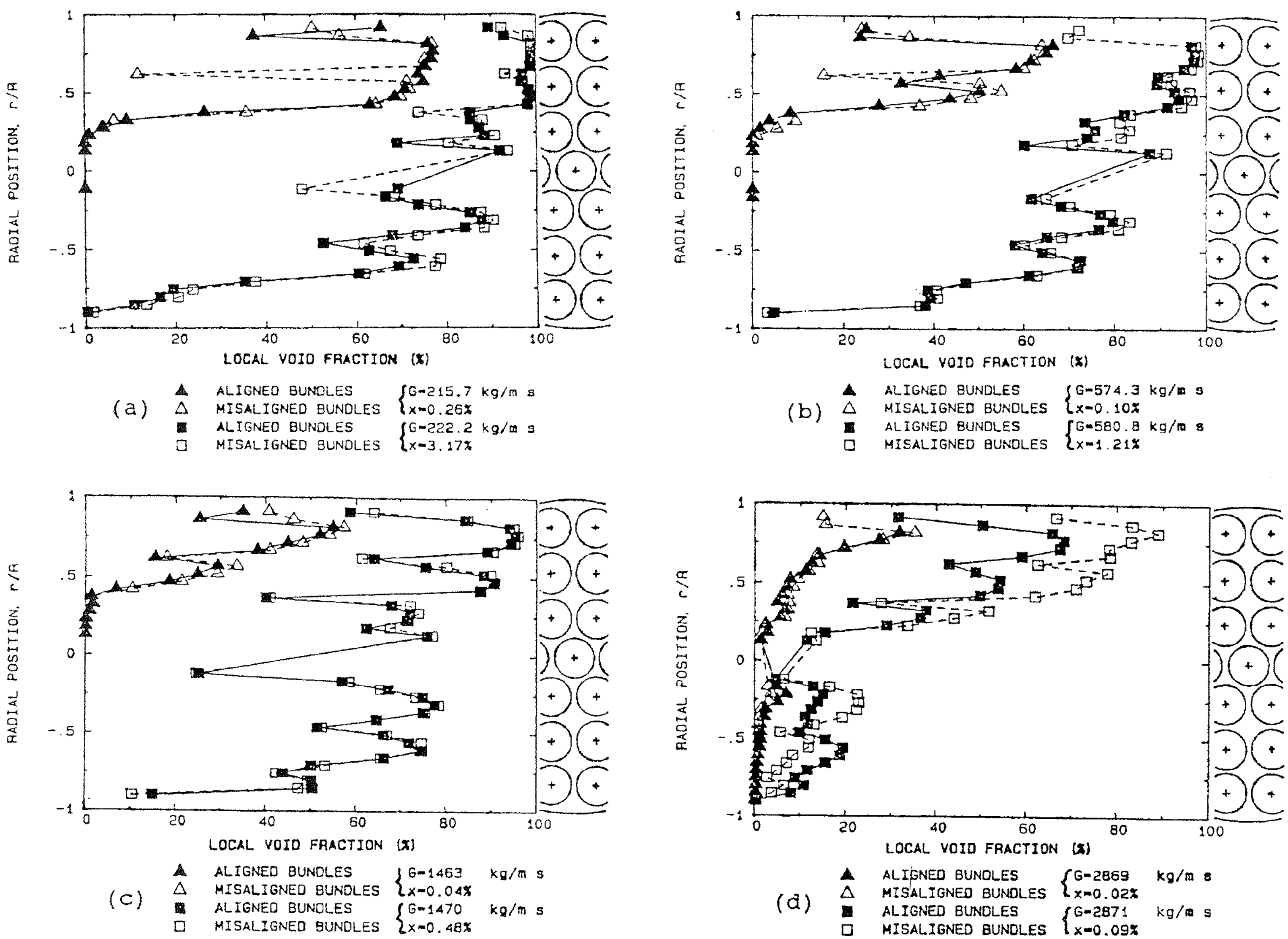

Figure 7: Void Distributions in Aligned and Misaligned 37-Rod Bundles at Various Mass Fluxes and Qualities.

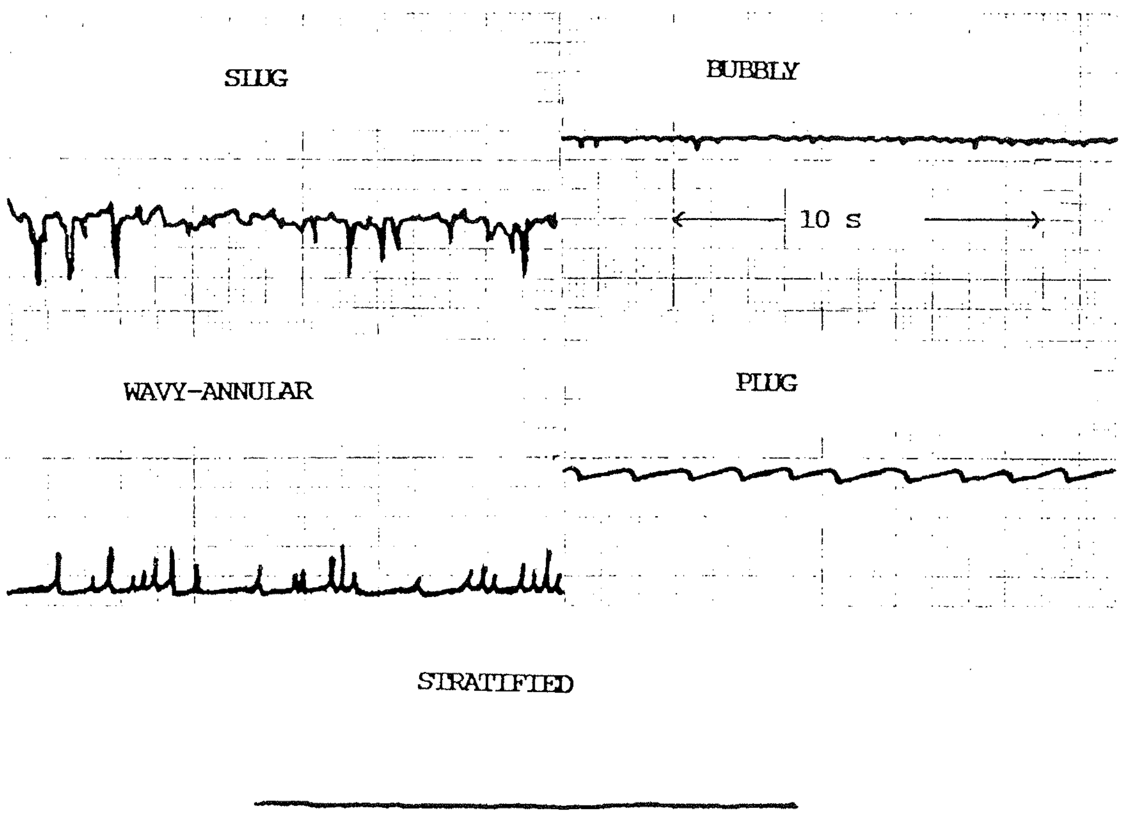

Figure 8: Waveform Signals of Instrumented Top Element of a 37-Rod Bundle for Various Flow Regimes.

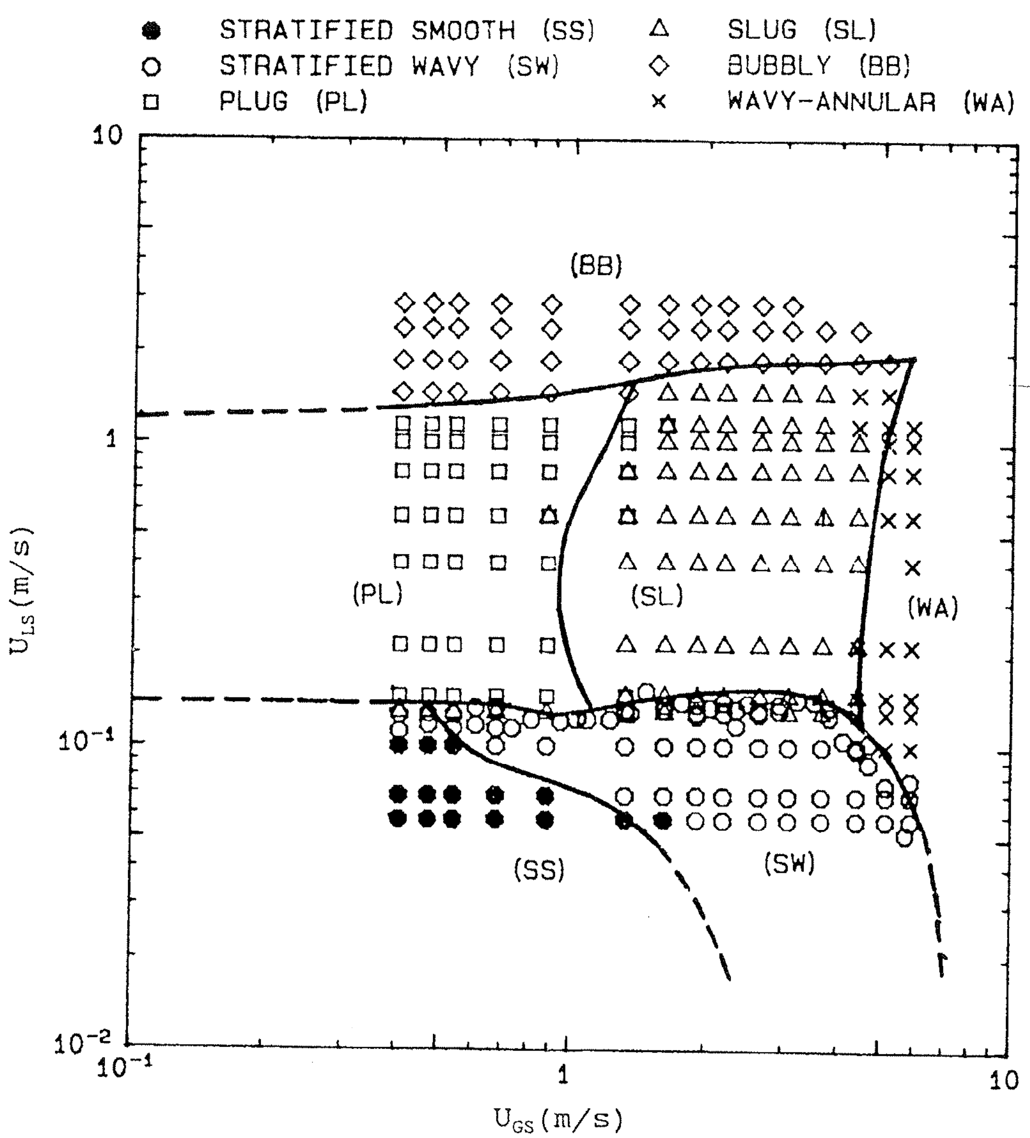

Figure 9: Horizontal Air-Water Flow-Regime Map for 37-Rod Bundles Based on Superficial Velocities at Room Temperature and Atmospheric Pressure.

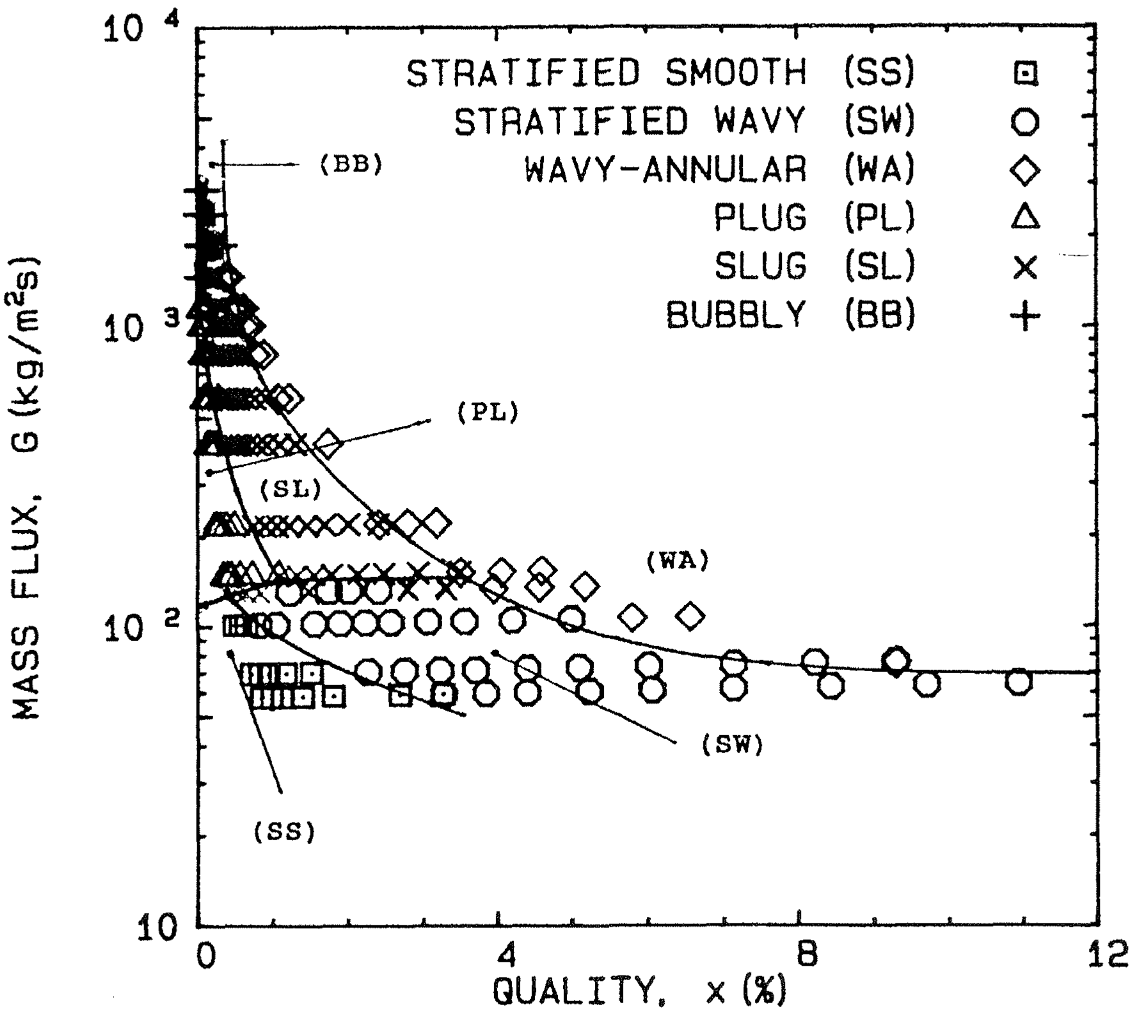

Figure 10: Horizontal Air-Water Flow-Regime Map for 37-Rod Bundles Based on Mass Flux and Quality at Room Temperature and Atmospheric Pressure.

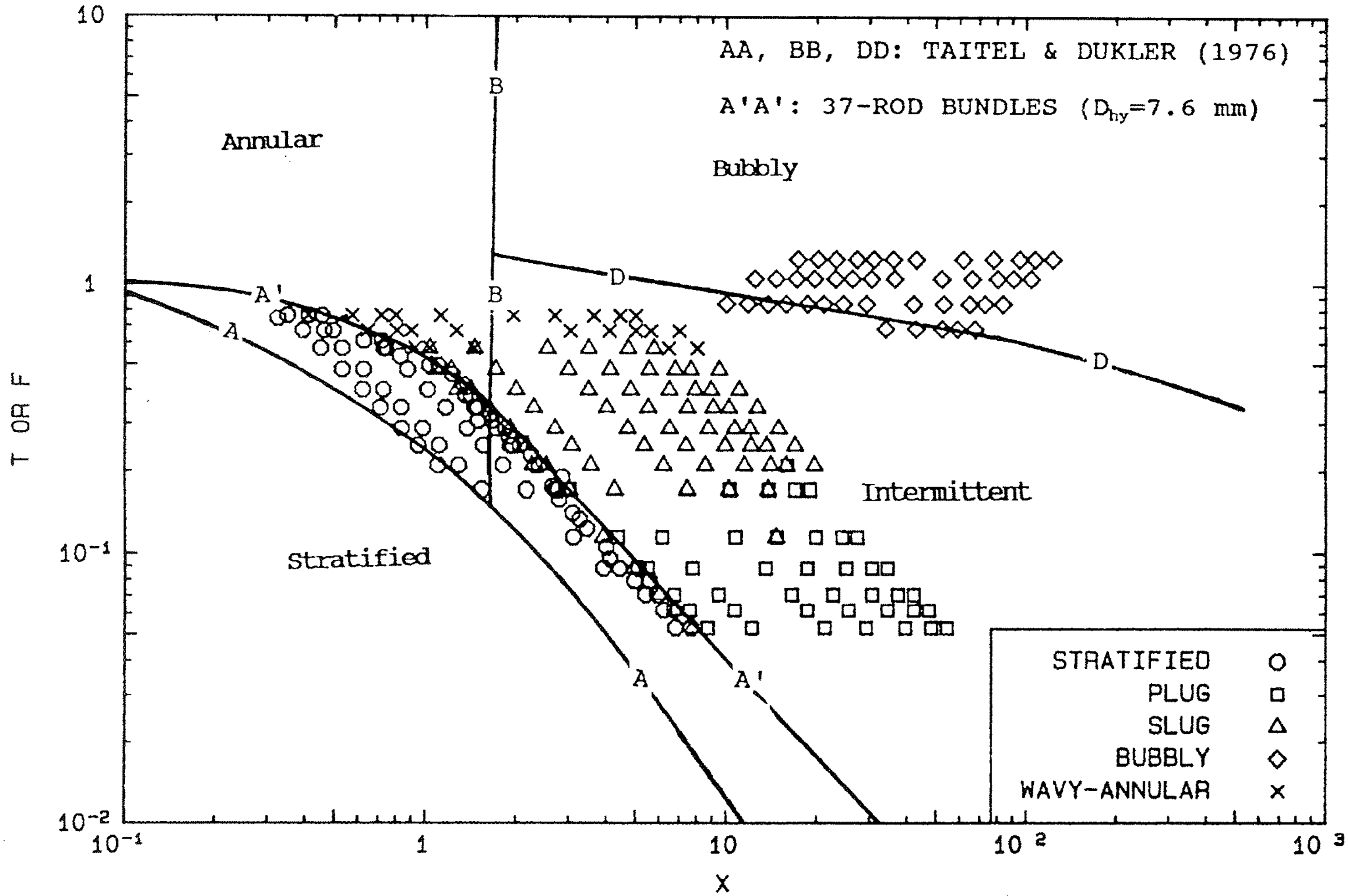

Figure 11: Generalized Flow-Regime Maps for Horizontal Pipes and 37-Rod Bundles.

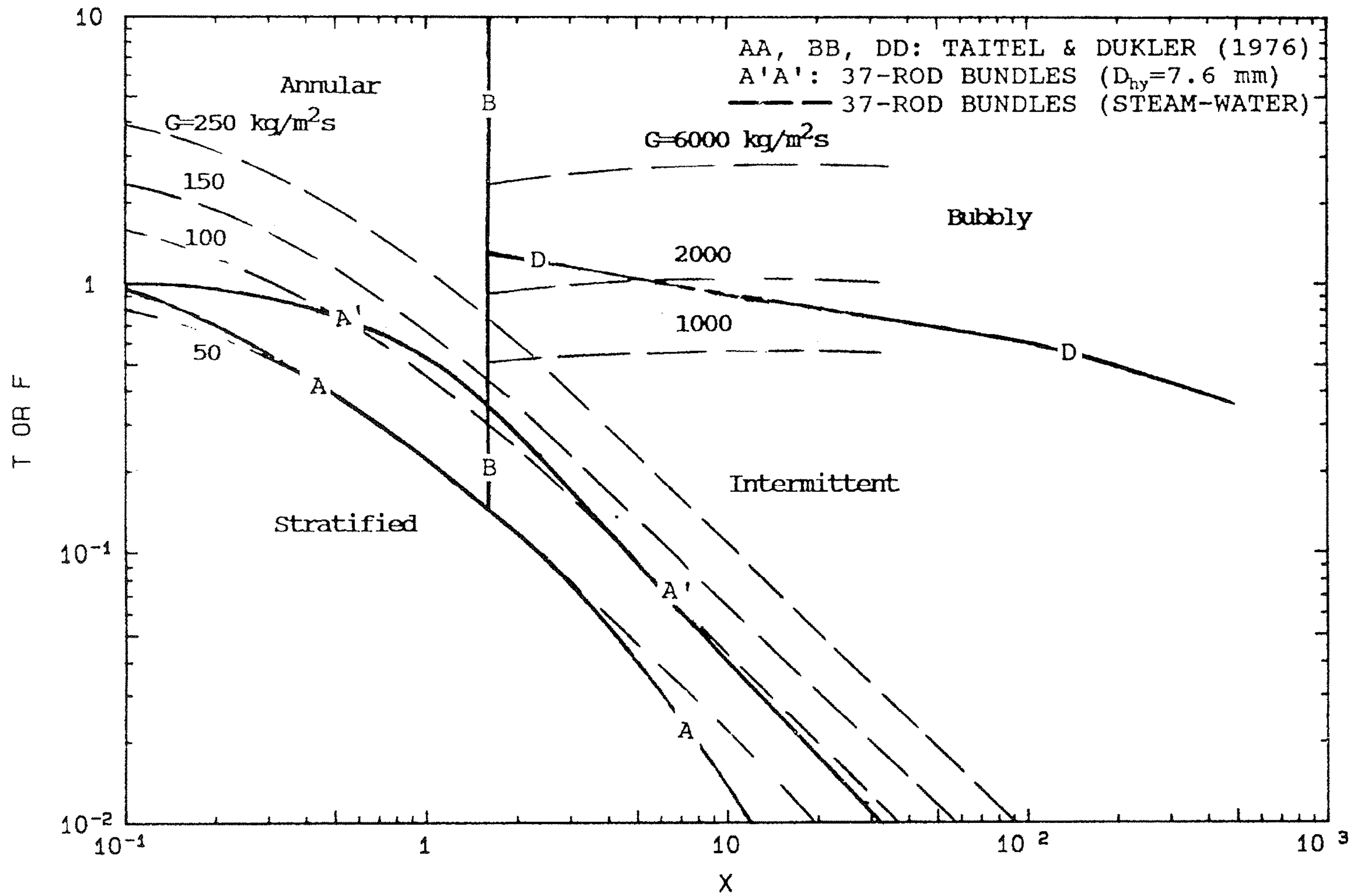

Figure 12: Generalized Flow-Regime Maps for Horizontal Pipes and 37-Rod Bundles Compared with Constant Mass Flux Lines of 10 MPa Steam-Water Flows in 37-Rod Bundles.

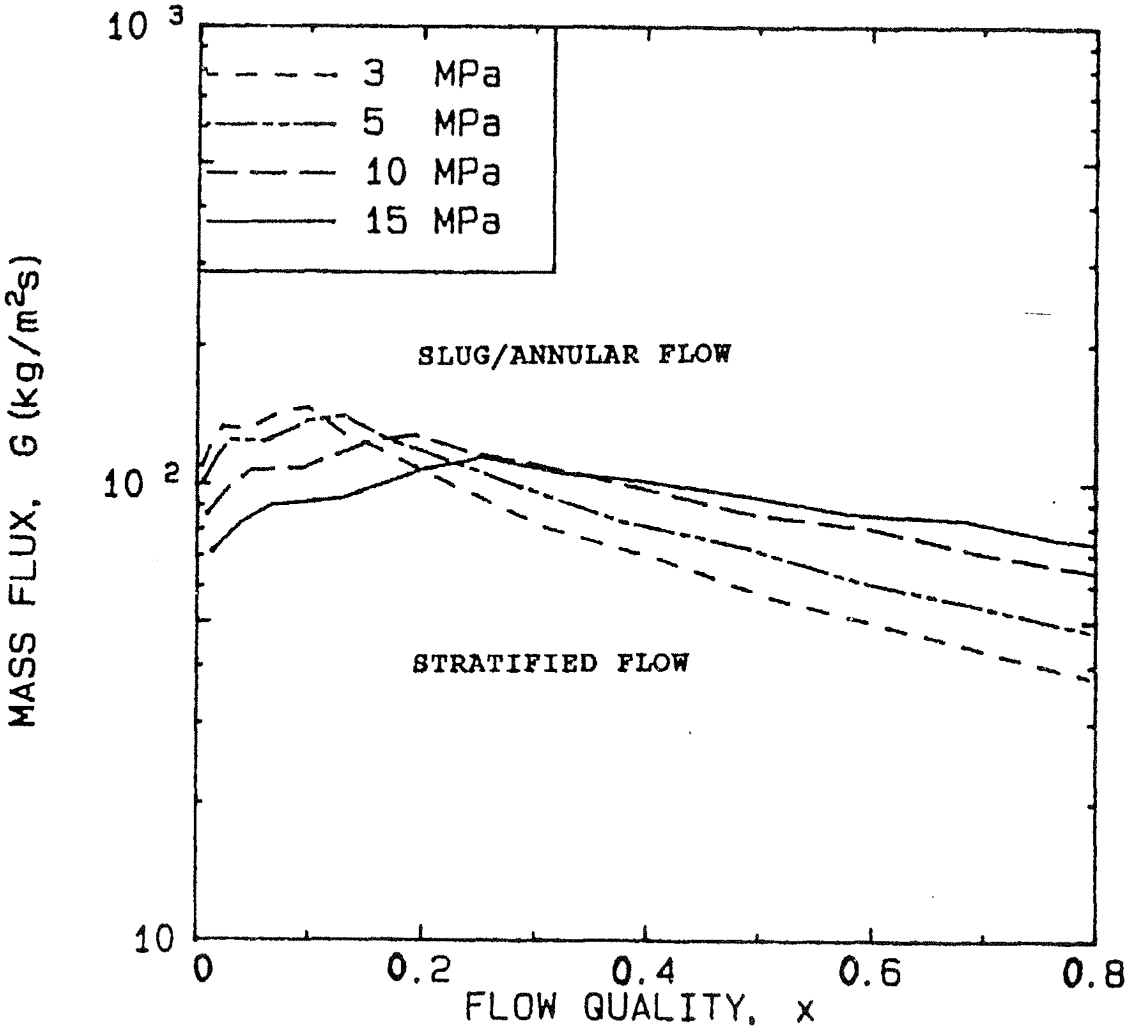

Figure 13: Flow Stratification in 37-Rod Bundle Steam-Water Flows at Various Pressures.